Journal of Computational Physics 231 (2012) 4823–4835

Contents lists available at SciVerse ScienceDirect

Journal of Computational Physics

journal homepage: www.elsevier.com/locate/jcp

Object-oriented electrodynamic *S*-matrix code with modern applications

Alex J. Yuffa *, John A. Scales

Department of Physics, Colorado School of Mines, Golden, CO 80401, USA

ARTICLE INFO

Article history:
Received 27 October 2011
Received in revised form 29 March 2012
Accepted 30 March 2012
Available online 16 April 2012

Keywords:
Wave propagation
Electromagnetic scattering
S-matrix method
Transfer matrix method
Negative refractive material

ABSTRACT

The *S*-matrix algorithm for the propagation of an electromagnetic wave through planar stratified media has been implemented in a modern object-oriented programing language. This implementation is suitable for the study of such applications as the Anderson localization of light and super-resolution (perfect lensing). For our open-source code to be as useful as possible to the scientific community, we paid particular attention to the pathological cases that arise in the limit of vanishing absorption.

1. Introduction

Electromagnetic wave propagation through planar stratified media (multilayer stack) is a century old problem in physics [1,2]. It may be somewhat surprising that it is still relevant today. In fact, it has only relatively recently been discovered that the transmission and reflection coefficients for a multilayer stack may be written down without any computations by using a complex version of the elementary symmetric functions [3,4]. It has also been recently discovered that the complex reflection coefficients follow the generalized version of the composition law used to add parallel velocities in the theory of special relativity, see [5,6] and Refs. within. It is possible to use the aforementioned properties to formulate a numerical wave propagation algorithm in planar stratified media as was done in [7], yet the resulting algorithm appears to be numerically unstable. The more traditional approach of the late 1940s, namely, the transfer matrix algorithm [8–11], is also numerically unstable. Both algorithms are numerically unstable because they contain exponentially increasing and decreasing terms, see Section 5. There also exists an *R*-matrix algorithm [12–15], but it is only conditionally stable (for reasons different from above) [12,15]. We use a simple version of the *S*-matrix algorithm, which is numerically stable [15–19]. Before considering the details of the *S*-matrix algorithm and the need for its open-source implementation in a modern object-oriented language, we briefly mention some of the current applications we had in mind when we wrote the code.

In 1968, Veselago [20] considered a hypothetical non-active material in which the real parts of the permittivity and permeability are simultaneously negative; we refer to such a material as a *left-handed material* (LHM), but it is also known as a *negative refractive material*. It was only in the early 2000s that such an artificial material was fabricated [21,22], leading to an explosion of papers on the LHM, see [23] and Refs. within. One of the intriguing properties of the LHM is the ability to image with a sub-wavelength image resolution (super-resolution if you will), which has been proposed and studied in the context of a multilayer stack [24,25]. Another general area of application is the Anderson localization of light [26,27], which has been

* Corresponding author.
E-mail address: ayuffa@gmail.com (A.J. Yuffa).
URL: http://mesoscopic.mines.edu (J.A. Scales).

0021-9991/$ - see front matter © 2012 Elsevier Inc. All rights reserved.
http://dx.doi.org/10.1016/j.jcp.2012.03.018

studied both theoretically and experimentally by Scales et al. [28], who considered wave propagation at normal incidence through a multilayer stack made of quartz and Teflon wafers. The effects of total internal reflection on light localization in a random multilayer stack at oblique incidence have also been studied under the assumption of complete phase randomization [29] along with the effects of the LHM on localization [30]. Other applications include the study of asymmetrical properties of light in a Fabry-Pérot interferometer [31,32].

In all of the above applications, the *S*-matrix algorithm was or could have been used; however, to the best of our knowledge, an open-source and object-oriented implementation of the *S*-matrix algorithm suitable for the LHM as well as the right-handed material (RHM) (where the real parts of the permittivity and permeability are *not* simultaneously negative) is currently unavailable. Almost certainly, there are many "in-house" implementations of some version of the algorithms discussed above being passed around among colleagues. We suspect that some users of these "in-house" algorithms may be unaware of the numerical stability issues and of pathological cases where the numerical implementation is not clear, as discussed in Section 3. Moreover, in the context of reproducibility of scientific work, it is important to have an open-source and publicly available implementation.

This paper is self-contained as much as possible in order for our implementation of the *S*-matrix algorithm to be useful to the widest possible scientific community. We also point out the benefits and drawbacks of using a high-level programing language called Python for implementing our code, see Section 9.

2. Background

The source-free macroscopic Maxwell equations with assumed harmonic time dependence, $\exp(-i\omega t)$, in the Système International (SI) unit system, at every ordinary point in space, are:

$$\nabla\cdot\mathbf{D}=0,\quad \nabla\cdot\mathbf{B}=0, \tag{1a}$$

$$\nabla\times\mathbf{E}=i\omega\mathbf{B},\quad \nabla\times\mathbf{H}=-i\omega\mathbf{D}, \tag{1b}$$

where $\mathbf{E}$ is the electric field, $\mathbf{D}$ is the displacement field, $\mathbf{B}$ is the magnetic field, $\mathbf{H}$ is the magnetic intensity, and ω is the angular frequency. By an ordinary point in space, we mean a point in space in whose "neighborhood" the physical properties of the medium are continuous. Thus, strictly speaking, one cannot apply Maxwell's equations at a surface that separates two physically different media. If the medium is isotropic and homogeneous, then $\mathbf{D}=\epsilon\mathbf{E}$ and $\mathbf{B}=\mu\mathbf{H}$, where ϵ and μ are the permittivity and the permeability, respectively. Permittivity must satisfy the Kramers–Kronig relations and is therefore a complex-valued function of angular frequency. The same is true for permeability. Thus, in general, we have $\epsilon=\epsilon(\omega)\in\mathbb{C}$ and $\mu=\mu(\omega)\in\mathbb{C}$.

The source-free macroscopic Maxwell equations are first-order linear partial differential equations (PDEs) that must be supplemented by some boundary conditions. The conventional boundary conditions for a source-free interface separating two media (1 and 2) are:

$$\mathbf{n}\cdot\left(\mathbf{D}^{(2)}-\mathbf{D}^{(1)}\right)=0,\quad \mathbf{n}\cdot\left(\mathbf{B}^{(2)}-\mathbf{B}^{(1)}\right)=0, \tag{2a}$$

$$\mathbf{n}\times\left(\mathbf{E}^{(2)}-\mathbf{E}^{(1)}\right)=\mathbf{0},\quad \mathbf{n}\times\left(\mathbf{H}^{(2)}-\mathbf{H}^{(1)}\right)=\mathbf{0}, \tag{2b}$$

where $\mathbf{n}$ is a unit normal to the interface, and the superscript on the fields indicates from which medium the interface is approached.

Taking the curl of (1b), then simplifying the result using the $\nabla\times(\nabla\times\mathbf{A})=\nabla(\nabla\cdot\mathbf{A})-\nabla^2\mathbf{A}$ vector identity and (1a), we obtain the vector Helmholtz equation within each layer

$$\left(\nabla^2+k^2\right)\left\{\begin{matrix}\mathbf{E}\\ \mathbf{H}\end{matrix}\right\}=\mathbf{0}, \tag{3}$$

where k is the complex wavenumber, and $k^2=\mu\epsilon\omega^2$. In general, $k^2\neq kk^*$, where * denotes the complex conjugate, and the computation of k from k^2 must be done with extreme care. For example, the permittivity and permeability for an absorbing material are taken to be $\epsilon=\epsilon'+i\epsilon''$ and $\mu=\mu'+i\mu''$, respectively, where $\{\epsilon',\mu'\}\in\mathbb{R}$, $\{\epsilon',\mu''\}\in\mathbb{R}^+$ and $\mathbb{R}^+$ denotes the positive real numbers.[1] Let $\epsilon=|\epsilon|e^{i\theta_\epsilon}$ and $\mu=|\mu|e^{i\theta_\mu}$, where $\{\theta_\epsilon,\theta_\mu\}\in[0,\pi]$.[2] Then

$$k^2=\epsilon\mu\omega^2$$

$$k=\sqrt{|\epsilon||\mu|}\omega e^{i\left(\frac{\theta_\epsilon+\theta_\mu+2\pi n}{2}\right)},\quad n=0,1, \tag{4}$$

where $\omega>0$. The choice of the root in (4) is dictated by the physical requirement that, in an absorbing medium, the wave must decay and not exponentially grow. Let $k=k'+ik''$, $\{k',k''\}\in\mathbb{R}$. Without loss of generality, consider a plane wave

[1] For the $\exp(+i\omega t)$ time dependence, $\epsilon=\epsilon'-i\epsilon''$, $\mu=\mu'-i\mu''$, where $\{\epsilon',\mu'\}\in\mathbb{R}$, $\{\epsilon'',\mu''\}\in\mathbb{R}^+$.

[2] We always mean the *positive* square root of x when we write $\sqrt{x}$, where $x\in\mathbb{R}^+$. The fundamental issue with the $w=z^{\frac{1}{2}}$ mapping is that the "square root" function has *branch points* at $z=0$ and $z=\infty$ and thus must have a *branch cut* connecting the two branch points, see [51, vol. 1, Section 54].

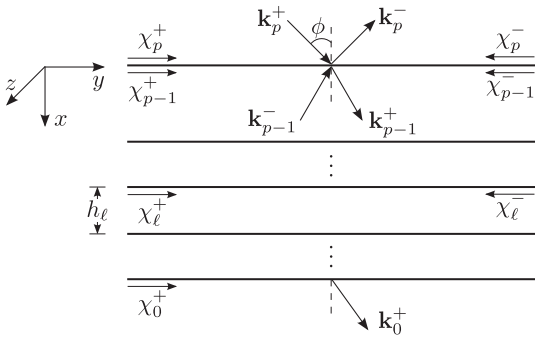

Fig. 1. The cross-sectional view of the multilayer stack is shown. The multilayer stack consists of $p+1$ regions made of a RHM. A parallel polarized wave is incident from a semi-infinite ambient medium (region p). The origin of the coordinate system is set on the planar interface separating regions p and $p-1$. The 0th region is a semi-infinite substrate.

propagating in the *positive* x-direction; then, we have $e^{i(kx-\omega t)} = e^{-k''x}e^{i(k'x-\omega t)}$. Therefore, k'' must be *greater than zero* in order for the wave to decay in the positive x-direction.

2.1. Pathological cases at normal incidence

In the case of a perfect dielectric ($\epsilon'' = 0$ and $\mu'' = 0$), the rule for choosing a physically appropriate root in (4) may be established by taking the limit as absorption goes to zero.

Consider an almost perfect dielectric made of the RHM. Let $\epsilon = |\epsilon|e^{i\theta_\epsilon}$, $\mu = |\mu|e^{i\theta_\mu}$, where θ_ϵ and θ_μ are infinitesimally small *positive* numbers, then $\frac{\theta_\epsilon+\theta_\mu}{2} \ll \pi$ and $\frac{\theta_\epsilon+\theta_\mu}{2} + \pi > \pi$. Thus, we must choose the $n = 0$ root in (4), i.e., $k = \sqrt{|\epsilon||\mu|}e^{i\left(\frac{\theta_\epsilon+\theta_\mu}{2}\right)}\omega$. In the case of a truly perfect dielectric (at fixed frequency), we may take the limit as θ_ϵ and θ_μ approach zero to obtain $k = \sqrt{|\epsilon||\mu|}\omega$.

In the case of an almost perfect dielectric made of a LHM: Let $\epsilon = |\epsilon|e^{i\theta_\epsilon}$, $\mu = |\mu|e^{i\theta_\mu}$, where θ_ϵ and θ_μ are slightly *less than* π, then $\frac{\theta_\epsilon+\theta_\mu}{2} < \pi$ and $\frac{\theta_\epsilon+\theta_\mu}{2} + \pi > \pi$. Thus, we must again choose the $n = 0$ root in (4), i.e., $k = \sqrt{|\epsilon||\mu|}e^{i\left(\frac{\theta_\epsilon+\theta_\mu}{2}\right)}\omega$. For a truly perfect dielectric (at fixed frequency), we may take the limit as θ_ϵ and θ_μ approach π to obtain $k = \sqrt{|\epsilon||\mu|}e^{i\pi}\omega = -\sqrt{|\epsilon||\mu|}\omega$. Notice that for the LHM with zero absorption, $k < 0$, and for the RHM with zero absorption, $k > 0$.

3. Wave propagation in stratified media

Consider the three-dimensional space divided into $p+1$ regions. The regions are infinite in the yz-plane, see Fig. 1. The interfaces separating the regions are assumed to be perfectly planar (yz-plane). The regions $\ell = 0,\ldots,p-1$ are assumed to be isotropic and homogeneous with a complex permittivity, ϵ_ℓ, and complex permeability, μ_ℓ. The region p is assumed to be isotropic and homogeneous with real permittivity, ϵ_p, and real permeability, μ_p. In other words, we have $\{\epsilon_\ell, \mu_\ell\} \in \mathbb{C}$ for $\ell = 0,\ldots,p-1$ and $\{\epsilon_p, \mu_p\} \in \mathbb{R}$.

A monochromatic plane wave in the ℓth region is given by

$$\left\{\begin{matrix}\mathbf{E}_\ell(\mathbf{r},t)\\ \mathbf{H}_\ell(\mathbf{r},t)\end{matrix}\right\} = \left\{\begin{matrix}\mathbf{E}_\ell\\ \mathbf{H}_\ell\end{matrix}\right\}e^{i(\mathbf{k}_\ell\cdot\mathbf{r}-\omega t)}, \quad \ell = 0,\ldots,p, \tag{5}$$

where $\mathbf{r} = x\hat{\mathbf{x}} + y\hat{\mathbf{y}} + z\hat{\mathbf{z}}$, $\{\mathbf{E}_\ell, \mathbf{H}_\ell\}$ are the *complex* vector amplitudes, $\mathbf{k}_\ell = k_{x,\ell}\hat{\mathbf{x}} + k_{y,\ell}\hat{\mathbf{y}} + k_{z,\ell}\hat{\mathbf{z}}$ is the *complex* wavevector. It is clear that (5) satisfies (3) if

$$\mathbf{k}_\ell\cdot\mathbf{k}_\ell = k_{x,\ell}^2 + k_{y,\ell}^2 + k_{z,\ell}^2 = k_\ell^2 = \epsilon_\ell\mu_\ell\omega^2. \tag{6}$$

Without loss of generality, we can set $k_{z,\ell} = 0$ because we can always rotate the coordinate system so that the y-axis is parallel to the part of the $\mathbf{k}$ vector that lies in the yz-plane, see Fig. 1.[3] The solution given by (5) in each region must also satisfy the boundary conditions given by (2). Substituting (5) into (2) yields,

$$k_{y,p} = k_{y,\ell}, \quad \ell = 0,\ldots,p-1, \tag{7}$$

where $k_{y,p} \in \mathbb{R}$ because we have assumed that the region p has real permittivity and permeability. Therefore, from (7) we have $k_{y,\ell} \in \mathbb{R}$, but note that in general, $k_{x,\ell} \in \mathbb{C}$ for $\ell = 0,\ldots,p-1$. Using (6) and (7) yields

[3] We could have chosen to set $k_{y,\ell} = 0$, and then rotated the coordinate system so that the z-axis is parallel to the part of the $\mathbf{k}$ vector that lies in the yz-plane. The point is that $\mathbf{k}$ can always be made into a two-dimensional vector.

$$k_{x,\ell} = \left(\epsilon_\ell \mu_\ell \omega^2 - k_{y,p}^2\right)^{1/2} \text{ with } \mathrm{Im}[k_{x,\ell}] > 0 \tag{8}$$

for $\ell = 0,\ldots,p$, where Im denotes the imaginary part, and the root choice, $\mathrm{Im}[k_{x,\ell}] > 0$, is dictated by the decaying wave requirement, see Section 2.

3.1. Pathological cases at oblique incidence

It is clear from (8) that if $\epsilon_\ell'' = 0,\ \mu_\ell'' = 0$ and $\epsilon_\ell \mu_\ell \omega^2 > k_{y,p}^2$, then the root choice is not resolved by the $\mathrm{Im}[k_{x,\ell}] > 0$ requirement. In order to resolve the root choice, we proceed by taking a limit as absorption goes to zero just as we did in Section 2.1. For the RHM, let $\epsilon_\ell = |\epsilon_\ell| e^{i\theta_{\epsilon_\ell}},\ \mu_\ell = |\mu_\ell| e^{i\theta_{\mu_\ell}}$ and for the LHM, let $\epsilon_\ell = |\epsilon_\ell| e^{i(\pi-\theta_{\epsilon_\ell})},\ \mu_\ell = |\mu_\ell| e^{i(\pi-\theta_{\mu_\ell})}$, where θ_{ϵ_ℓ} and θ_{μ_ℓ} are infinitesimally small *positive* numbers. Then $k_{x,\ell}^2$ can be approximately written as $k_{x,\ell}^2 \approx |A| e^{\pm i\gamma}$, where $0 \leqslant \gamma \ll \pi,\ \lim_{\{\epsilon_\ell'', \mu_\ell''\} \to 0} \gamma = 0$, and the positive (negative) sign in the exponential corresponds to the RHM (LHM). Thus, we have

$$\mathrm{Im}[k_{x,\ell}] = \sqrt{|A|}\left\{\sin\left(\frac{\pm\gamma}{2}\right), \sin\left(\frac{\pm\gamma}{2} + \pi\right)\right\},$$

where it is clear that for the RHM (LHM) the first (second) root must be chosen in order for $\mathrm{Im}[k_{x,\ell}] > 0$. Therefore, if $\epsilon_\ell'' = 0,\ \mu_\ell'' = 0$ and $\epsilon_\ell \mu_\ell \omega^2 > k_{y,p}^2$, then for the RHM we have $k_{x,\ell} = +\sqrt{|\epsilon_\ell||\mu_\ell|\omega^2 - k_{y,p}^2}$, and for the LHM we have $k_{x,\ell} = -\sqrt{|\epsilon_\ell||\mu_\ell|\omega^2 - k_{y,p}^2}$.

3.2. Origin and numerical treatment of the pathologies

The limiting procedure carried out in Section 2.1 and 3.1 appears to be reasonable, but unfortunately, it is also not physically attainable, even in principle! If we view $\epsilon(\omega)$ and $\mu(\omega)$, where $\omega = \omega' + i\omega''$, in the context of the Kramers–Kronig relations, then $\epsilon(\omega)$ and $\mu(\omega)$ are analytic functions in the upper-half ω-plane. Furthermore, it can be shown that $\epsilon(\omega)$ and $\mu(\omega)$ are never purely real for any finite ω except for $\omega' = 0$ (positive imaginary axis), e.g., see [33, Section 123] and [34, Section 82]. Therefore, the common practice of replacing $\epsilon' + i\epsilon''$ by ϵ' and $\mu' + i\mu''$ by μ' even in an infinitesimally small ω' interval *cannot* be justified. Moreover, by considering the *global* behavior of $k_{x,\ell}$ it can be shown that for a non-active medium $k_{x,\ell}$ is never zero [35]. However, we see from (8) that $k_{x,\ell}$, for any $\ell \neq p$ may be equal to zero if ϵ_ℓ and μ_ℓ are purely real. Of course, this case only occurs when the angle of incidence precisely equals one of the critical angles, and from the global properties of ϵ and μ we see that such angles *cannot* exist.

The above discussion suggests that the pathological cases only occur in an *unphysical* approximation, i.e., $\epsilon \approx \epsilon'$ and $\mu \approx \mu'$. In our numerical code, the user may select how to deal with the pathologies from the following two schemes:

1. If a region contains purely real permittivity and permeability, then the real permittivity and permeability are replaced by a slightly absorbing permittivity and permeability, respectively, i.e., for $\ell \neq p,\ \epsilon_\ell' \to \epsilon_\ell' + i\epsilon_\ell''$ and $\mu_\ell' \to \mu_\ell' + i\mu_\ell''$, where ϵ_ℓ'' and μ_ℓ'' are small positive numbers.
2. If a region contains purely real permittivity and permeability, then the $k_{x,\ell}$ is computed as describe in Section 2.1 and 3.1. If this scheme is chosen, then the code may produce erroneous results at or very near the critical angles.

4. Polarization

The most general polarization state is an *elliptical* polarization state. However, there is no need to consider this general case because an elliptical polarization state can always be decomposed into a linear combination of two linearly independent polarization states, namely, the *parallel* polarization state and the *perpendicular* polarization state. In what follows, it is convenient to express $\mathbf{E}_\ell(\mathbf{r}, t)$ and $\mathbf{H}_\ell(\mathbf{r}, t)$ in terms of each other by substituting (5) into (1b) (with $\mathbf{D}_\ell = \epsilon_\ell \mathbf{E}_\ell$) and using the vector identity

$$\nabla \times \left\{\begin{matrix}\mathbf{E}_\ell(\mathbf{r}, t)\\ \mathbf{H}_\ell(\mathbf{r}, t)\end{matrix}\right\} = i\mathbf{k}_\ell \times \left\{\begin{matrix}\mathbf{E}_\ell\\ \mathbf{H}_\ell\end{matrix}\right\} e^{i(\mathbf{k}_\ell \cdot \mathbf{r} - \omega t)}$$

to obtain

$$\mathbf{E}_\ell(\mathbf{r}, t) = -\frac{\mathbf{k}_\ell \times \mathbf{H}_\ell(\mathbf{r}, t)}{\epsilon_\ell \omega}, \tag{9a}$$

$$\mathbf{H}_\ell(\mathbf{r}, t) = \frac{\mathbf{k}_\ell \times \mathbf{E}_\ell(\mathbf{r}, t)}{\mu_\ell \omega}. \tag{9b}$$

4.1. Parallel polarization

A monochromatic plane wave is said to have parallel polarization if the electric field is parallel to the *plane of incidence*. The plane of incidence is defined by the wavevector $\mathbf{k}$ and the normal vector to the surface $\mathbf{n}$; i.e., $\mathbf{k}$ and $\mathbf{n}$ lie in the plane of incidence. From Fig. 1, we have $\mathbf{k}$ in the xy-plane and $\mathbf{n} = \pm\hat{\mathbf{x}}$, thus, the plane of incidence is the xy-plane.

Consider a parallel polarized incident plane wave of angular frequency ω propagating in the *positive x*-direction. Maxwell's equation (1) are linear PDEs, thus, the total wave inside each region may be decomposed into reflected and transmitted waves with the following wavevectors:

$$\mathbf{k}_\ell^\pm = \pm k_{x,\ell}\hat{\mathbf{x}} + k_{y,\ell}\hat{\mathbf{y}}, \tag{10}$$

where $k_{x,\ell}$ is given by (8), $k_{y,\ell}$ is given by (7), $^+$ indicates a transmitted wave propagating in the $+x$-direction, and $^-$ indicates a reflected wave propagating in the $-x$-direction; notice that there is no reflected wave in the 0th region, see Fig. 1. The magnetic intensity in each region is given by

$$\mathbf{H}_\ell^\pm(\mathbf{r},t) = \epsilon_\ell \omega E_\ell^\pm \exp\left[\mathrm{i}\left(\mathbf{k}_\ell^\pm \cdot \mathbf{r} - \omega t\right)\right]\hat{\mathbf{z}}, \tag{11}$$

where E_ℓ^+ is the *complex* amplitude associated with the transmitted wave, E_ℓ^- is the *complex* amplitude associated with the reflected wave, and $E_{\ell=0}^- \equiv 0$. Substituting (11) into (9a) yields

$$\mathbf{E}_\ell^\pm(\mathbf{r},t) = E_\ell^\pm \exp\left[\mathrm{i}\left(\mathbf{k}_\ell^\pm \cdot \mathbf{r} - \omega t\right)\right]\left[-k_{y,\ell}\hat{\mathbf{x}} \pm k_{x,\ell}\hat{\mathbf{y}}\right]. \tag{12}$$

From (2b), we see that the *y*-component of the total electric field and the total magnetic intensity are continuous across the interface. It is convenient to define a new symbol for the *y*-component of the electric field evaluated on the interface. Let

$$\chi_\ell^\pm = \pm k_{x,\ell} E_\ell^\pm \exp\left[\pm \mathrm{i} k_{x,\ell} \sum_{s=\ell+1}^{p} h_s\right], \tag{13}$$

where h_ℓ is the thickness of the ℓth region and, for convenience, we set $h_{\ell=0} = h_{\ell=p} \equiv 0$. In (13), $\chi^\pm_{\ell=0,\ldots,p-1}$, denotes the *y*-component of the electric field at the interface between regions $\ell$and $\ell+1$ (the interface is approached from the ℓth region), and $\chi^\pm_{\ell=p}$ denotes the *y*-component of the electric field at the interface between regions p and $p-1$ (the interface is approached from region p), see Fig. 1. Substituting (11) and (12) into (2b), and using (13) to simplify the result, yields

$$\mathrm{e}^{+\mathrm{i}k_{x,\ell+1}h_{\ell+1}}\chi_{\ell+1}^+ + \mathrm{e}^{-\mathrm{i}k_{x,\ell+1}h_{\ell+1}}\chi_{\ell+1}^- = \chi_\ell^+ + \chi_\ell^-, \tag{14a}$$

$$w_{\ell+1}\left(e^{+\mathrm{i}k_{x,\ell+1}h_{\ell+1}}\chi_{\ell+1}^+ - \mathrm{e}^{-\mathrm{i}k_{x,\ell+1}h_{\ell+1}}\chi_{\ell+1}^-\right) = w_\ell\left(\chi_\ell^+ - \chi_\ell^-\right), \tag{14b}$$

for $\ell = 0,\ldots,p-1$, where

$$w_\ell = \frac{\epsilon_\ell \omega}{k_{x,\ell}}, \quad \ell = 0,\ldots,p. \tag{15}$$

After we obtain a linear system for the perpendicular polarization case, we will solve the linear system given by (14), see Section 5.

4.2. Perpendicular polarization

A monochromatic plane wave is said to have perpendicular polarization if the electric field is perpendicular to the *plane of incidence*. The electric field in each region is given by

$$\mathbf{E}_\ell^\pm(\mathbf{r},t) = E_\ell^\pm \exp\left[\mathrm{i}\left(\mathbf{k}_\ell^\pm \cdot \mathbf{r} - \omega t\right)\right]\hat{\mathbf{z}}, \tag{16}$$

where $\mathbf{k}_\ell^\pm$ is given by (10), and the $^\pm$ superscripts have the same meaning as in Section 4.1. Also as in Section 4.1, we set $E_{\ell=0}^- \equiv 0$ because there is no reflected wave in the 0th region. Substituting (16) into (9b) yields

$$\mathbf{H}_\ell^\pm(\mathbf{r},t) = \frac{E_\ell^\pm}{\mu_\ell \omega} \exp\left[\mathrm{i}\left(\mathbf{k}_\ell^\pm \cdot \mathbf{r} - \omega t\right)\right]\left[k_{y,\ell}\hat{\mathbf{x}} \mp k_{x,\ell}\hat{\mathbf{y}}\right]. \tag{17}$$

From (2b), we see that both the total electric field and the *y*-component of the total magnetic intensity are continuous across the interface. Let the electric field evaluated on the interface be denoted by

$$\chi_\ell^\pm = E_\ell^\pm \exp\left[\pm \mathrm{i} k_{x,\ell} \sum_{s=\ell+1}^{p} h_s\right], \tag{18}$$

where $\chi^\pm_{\ell=0,\ldots,p-1}$ denotes the *z*-component of the electric field at the interface between regions $\ell$and ł + 1 (the interface is approached from the ℓth region) and $\chi^\pm_{\ell=p}$ denotes the *z*-component of the electric field at the interface between regions p and $p-1$ (the interface is approached from region p). Substituting (16) and (17) into (2b), and using (18) to simplify the result, yields (14), where

$$w_\ell = -\frac{k_{x,\ell}}{\mu_\ell \omega}, \quad \ell = 0,\ldots,p. \tag{19}$$

Notice that the linear system for the perpendicular polarization case is the same as the linear system for the parallel polarization case, but the definitions of $\chi_\ell^\pm$ and w_ℓ are different.

5. Linear system

The traditional approach to solving the linear system given by (14) is to rewrite it as

$$\begin{bmatrix} \chi_{\ell+1}^+ \\ \chi_{\ell+1}^- \end{bmatrix} = M_\ell \begin{bmatrix} \chi_\ell^+ \\ \chi_\ell^- \end{bmatrix}, \quad \ell = 0, \ldots, p-1, \tag{20a}$$

where

$$M_\ell = \frac{1}{2w_{\ell+1}} \begin{bmatrix} (w_{\ell+1}+w_\ell)\psi_{\ell+1}^{-1} & (w_{\ell+1}-w_\ell)\psi_{\ell+1}^{-1} \\ (w_{\ell+1}-w_\ell)\psi_{+1} & (w_{\ell+1}+w_\ell)\psi_{\ell+1} \end{bmatrix}, \tag{20b}$$

and $\psi_\ell = \exp(\mathrm{i}k_{x,\ell}h_\ell)$. To compute χ_0^+, we iterate (20a) until $\ell = p-1$ to obtain

$$\begin{bmatrix} \chi_p^+/\chi_0^+ \\ \chi_p^-/\chi_0^+ \end{bmatrix} = M_{p-1}M_{p-2}\ldots M_0 \begin{bmatrix} 1 \\ 0 \end{bmatrix}. \tag{21}$$

After computing χ_0^+ from (21), we can find $\chi_\ell^\pm$ from (20a). The approach outlined above is the standard transfer matrix method, but unfortunately it is numerically unstable because the top half of M_ℓ grows exponentially and the bottom half of M_ℓ decreases exponentially if $\mathrm{Im}[k_{x,\ell}h_\ell] \neq 0$. To avoid the numerical instability, we must reformulate the linear system given by (14) in terms of ψ_ℓ or ψ_ℓ^{-1} alone. If $\mathrm{Im}[k_{x,\ell}h_\ell]$ is large, then ψ_ℓ may cause underflow errors and ψ_ℓ^{-1} may cause overflow errors. Generally speaking, underflow is preferred to overflow because when underflow occurs, the (normal) number is rounded to the nearest subnormal number or to 0.0; thus, it is desirable to reformulate the linear system in terms of ψ_ℓ instead of ψ_ℓ^{-1} (see Section 5.1).

5.1. S-matrix

In this section, we present a particularly simple version of the S-matrix formulation of (14) that avoids numerical instabilities. To derive the S-matrix, we write a scattering matrix (S-matrix) for an "aggregate layer" consisting of $0,\ldots,\ell$ layers to obtain

$$\begin{bmatrix} \chi_\ell^- \\ \chi_0^+ \end{bmatrix} = \begin{bmatrix} s_\ell^{(1,1)} & s_\ell^{(1,2)} \\ s_\ell^{(2,1)} & s_\ell^{(2,2)} \end{bmatrix} \begin{bmatrix} 0 \\ \chi_\ell^+ \end{bmatrix}. \tag{22}$$

Using (20) to eliminate $\chi_\ell^\pm$ from (22) and comparing the result to (22) with $\ell \to \ell+1$ yields

$$s_{\ell+1}^{(1,2)} = \frac{w_{\ell+1} - w_\ell\left[1 - s_\ell^{(1,2)}\right]\left[1 + s_\ell^{(1,2)}\right]^{-1}}{w_{\ell+1} + w_\ell\left[1 - s_\ell^{(1,2)}\right]\left[1 + s_\ell^{(1,2)}\right]^{-1}}\psi_{\ell+1}^2, \tag{23a}$$

$$s_{\ell+1}^{(2,2)} = \frac{2w_{\ell+1}s_\ell^{(2,2)}}{w_{\ell+1}\left[1 + s_\ell^{(1,2)}\right] + w_\ell\left[1 - s_\ell^{(1,2)}\right]}\psi_{\ell+1}, \tag{23b}$$

for $\ell = 0,\ldots,p-1$, where $s_0^{(1,2)} = 0$ and $s_0^{(2,2)} = 1$. Substituting $\ell = p$ into (22) yields $\chi_0^+/\chi_p^+ = s_p^{(2,2)}$, where $s_p^{(2,2)}$ is computed recursively from (23b). Using (20) to compute $\chi_\ell^\pm$ would make the algorithm numerically unstable. To avoid introducing numerical instability in the computation of $\chi_\ell^\pm$, we eliminate χ_0^+ and $\chi_{\ell+1}^-$ from (20) and (22) to obtain

$$\chi_\ell^+ = \frac{2w_{\ell+1}\psi_{\ell+1}}{w_{\ell+1}\left[1 + s_\ell^{(1,2)}\right] + w_\ell\left[1 - s_\ell^{(1,2)}\right]}\chi_{\ell+1}^+, \tag{24a}$$

for $\ell = p-1,\ldots,0$ and

$$\chi_\ell^- = s_\ell^{(1,2)}\chi_\ell^+, \quad \ell = p,\ldots,1. \tag{24b}$$

Notice that $\chi_\ell^\pm$ only depends on $s_\ell^{(1,2)}$. The S-matrix algorithm is numerically stable because (23a) and (24) only depend on ψ_ℓ.

Originally, (23a) and (24) were derived in [16] by citing the general scattering-theory paradigm that requires existence of a linear relationship between χ_ℓ^- and χ_ℓ^+, i.e., $\chi_\ell^- = s_\ell^{(1,2)}\chi_\ell^+$, and then substituting it directly into (20) to obtain (23a) and (24a). Arguably our derivation is just as simple as in [16] but follows the traditional S-matrix formulation [15,17] more closely.

We would like to note that it is possible to formulate an S-matrix algorithm where $\chi_\ell^\pm$ are computed directly from χ_p^+ [18,19], but such a formulation requires recursive computation of *three* elements of an S-matrix rather than just *one* element

in our formulation. Moreover, it is also possible to obtain formulas that directly relate $\chi_\ell^\pm$ to χ_p^+ from our formulation by simply multiplying out (24), i.e., $\chi_\ell^+ = \tilde{s}_{\ell+1}^{(2,2)}\tilde{s}_{\ell+2}^{(2,2)}\cdots\tilde{s}_p^{(2,2)}\chi_p^+$ and $\chi_\ell^- = s_\ell^{(1,2)}\left(\tilde{s}_{\ell+1}^{(2,2)}\tilde{s}_{\ell+2}^{(2,2)}\cdots\tilde{s}_p^{(2,2)}\right)\chi_p^+$, where $\tilde{s}_{\ell+1}^{(2,2)} = s_{\ell+1}^{(2,2)}/s_\ell^{(2,2)}$.

6. Conserved quantities

In the case of the RHM, the time-averaged complex Poynting theorem for harmonic fields is given by

$$\nabla\cdot\mathbf{S} + Q^{(\mathrm{e})} + Q^{(\mathrm{m})} + 2\mathrm{i}\omega\left(u^{(\mathrm{e})} - u^{(\mathrm{m})}\right) = 0, \tag{25a}$$

where $\mathbf{S} = \frac{1}{2}\mathbf{E}\times\mathbf{H}^*$ is the complex Poynting vector and

$$u^{(\mathrm{e})} = \frac{\epsilon'}{4}\mathbf{E}\cdot\mathbf{E}^* = \frac{\epsilon'}{4}\|\mathbf{E}\|^2, \tag{25b}$$

$$u^{(\mathrm{m})} = \frac{\mu'}{4}\mathbf{H}\cdot\mathbf{H}^* = \frac{\mu'}{4}\|\mathbf{H}\|^2, \tag{25c}$$

$$Q^{(\mathrm{e})} = \frac{\omega\epsilon''}{2}\mathbf{E}\cdot\mathbf{E}^* = \frac{\omega\epsilon''}{2}\|\mathbf{E}\|^2, \tag{25d}$$

$$Q^{(\mathrm{m})} = \frac{\omega\mu''}{2}\mathbf{H}\cdot\mathbf{H}^* = \frac{\omega\mu''}{2}\|\mathbf{H}\|^2. \tag{25e}$$

In (25), $u^{(\mathrm{e})}$ is the *real* time-averaged electric density, $u^{(\mathrm{m})}$ is the *real* time-averaged magnetic density, $Q^{(\mathrm{e})}$ and $Q^{(\mathrm{m})}$ represent time-averaged electric and magnetic losses, respectively (e.g., Joule heating [36, Section 2.19, Section 2.20]). Substituting the total electric field and the total magnetic intensity into (25b) and (25c), respectively, yields

$$u_\ell^{(\mathrm{e})} = \frac{\epsilon'_\ell}{4}\left(\left\|\mathbf{E}_\ell^+\right\|^2 + \left\|\mathbf{E}_\ell^-\right\|^2 + 2\mathrm{Re}\left[\mathbf{E}_\ell^+\cdot\mathbf{E}_\ell^{-*}\right]\right), \tag{26a}$$

$$u_\ell^{(\mathrm{m})} = \frac{\mu'_\ell}{4}\left(\left\|\mathbf{H}_\ell^+\right\|^2 + \left\|\mathbf{H}_\ell^-\right\|^2 + 2\mathrm{Re}\left[\mathbf{H}_\ell^+\cdot\mathbf{H}_\ell^{-*}\right]\right), \tag{26b}$$

where Re denotes the real part.

In the case of the LHM, the complex Poynting theorem for harmonic fields given by (25) is *mathematically* correct. However, the identification of the real electric density (25b) and the real magnetic density (25c) is troublesome because both are *negative*. It was pointed out by Veselago [20] that the LHM must be accompanied by frequency dispersion, in which case the real electric density and the real magnetic density are not given by (25b) and (25c), respectively. Moreover, simultaneously negative permittivity and permeability occur very near resonance and there is therefore no frequency interval for the LHM where permittivity and permeability may be reasonably approximated by a constant. For a more detailed discussion see [23,37,38].

Another conserved quantity is the *fundamental invariant in multilayers* (FIM) [39,40], given by

$$w_{\ell+1}\left[\left(\psi_{\ell+1}\chi_{\ell+1}^+\right)^2 - \left(\psi_{\ell+1}^{-1}\chi_{\ell+1}^-\right)^2\right] = w_\ell\left[\left(\chi_\ell^+\right)^2 - \left(\chi_\ell^-\right)^2\right], \tag{27}$$

for $\ell = 0,\ldots,p-1$. The FIM is a product of the continuity conditions for the electric field (14a) and magnetic intensity (14b). However, the FIM is *not* an energy conservation statement because it contains $\left(\chi_\ell^\pm\right)^2$ and $\left(\chi_{\ell+1}^\pm\right)^2$ instead of $\left|\chi_\ell^\pm\right|^2$ and $\left|\chi_{\ell+1}^\pm\right|^2$. In our view, the FIM is particularly interesting because its structure is similar to that of the space-time interval of special relativity, $\mathrm{d}s^2 = \mathrm{d}x^2 - c^2\mathrm{d}t^2$, where c is the speed of light. Moreover, it has been pointed out in [41] that many results associated with wave propagation through planar stratified media are more easily derived through an analogy with special relativity. In this paper, we don't pursue the analogy between wave propagation though a multilayer stack and the theory of special relativity any further, but we do want to stress that this analogy is not a mere coincidence.

6.1. Energy densities for parallel polarization

It is convenient to introduce a new symbol for the transverse component (the y-component) of the electric field as a function of distance, x, into the multilayer stack. For $\ell = 0,\ldots,p$, let

$$\Gamma_\ell^\pm(x) = \pm k_{x,\ell}E_\ell^\pm\exp[\pm\mathrm{i}k_{x,\ell}x], \tag{28}$$

then,

$$\begin{aligned}\left|\Gamma_\ell^\pm(x)\right|^2 &= |k_{x,\ell}|^2\left|E_\ell^\pm\right|^2\exp\left(\mp 2\mathrm{Im}[k_{x,\ell}]x\right),\\ \mathrm{Re}\left[\Gamma_\ell^+(x)\Gamma_\ell^{-*}(x)\right] &= -|k_{x,\ell}|^2\mathrm{Re}\left[E_\ell^+E_\ell^{-*}\mathrm{e}^{+2\mathrm{i}\mathrm{Re}[k_{x,\ell}]x}\right].\end{aligned} \tag{29}$$

Substituting (12) into (26a) and using (29) to simplify the result yields

$$u_\ell^{(\mathrm{e})}(x) = \frac{\epsilon'_\ell}{4}\left[\left(1+\frac{k_{y,p}^2}{|k_{x,\ell}|^2}\right)\left(\left|\Gamma_\ell^+(x)\right|^2 + \left|\Gamma_\ell^-(x)\right|^2\right) + 2\left(1-\frac{k_{y,p}^2}{|k_{x,\ell}|^2}\right)\mathrm{Re}\left[\Gamma_\ell^+(x)\Gamma_\ell^{-*}(x)\right]\right]. \tag{30}$$

Substituting (11) into (26b) and using (29) to simplify the result yields

$$u_\ell^{(\mathrm{m})}(x) = \frac{\mu_\ell' |w_\ell|^2}{4}\left(\left|\Gamma_\ell^+(x)\right|^2 + \left|\Gamma_\ell^-(x)\right|^2 - 2\mathrm{Re}\left[\Gamma_\ell^+(x)\Gamma_\ell^{-*}(x)\right]\right), \tag{31}$$

where w_ℓ is given by (15).

6.2. Energy densities for perpendicular polarization

Again, it is convenient to introduce a new symbol for the transverse component (the z-component) of the electric field as a function of distance, x, into the multilayer stack. For $\ell = 0,\ldots,p$, let

$$\Gamma_\ell^\pm(x) = E_\ell^\pm \exp\left[\pm \mathrm{i} k_{x,\ell} x\right], \tag{32}$$

then,

$$\begin{aligned} \left|\Gamma_\ell^\pm(x)\right|^2 &= \left|E_\ell^\pm\right|^2 \exp\left(\mp 2\mathrm{Im}[k_{x,\ell}]x\right), \\ \mathrm{Re}\left[\Gamma_\ell^+(x)\Gamma_\ell^{-*}(x)\right] &= \mathrm{Re}\left[E_\ell^+ E_\ell^{-*} \mathrm{e}^{+2\mathrm{i}\mathrm{Re}[k_{x,\ell}]x}\right]. \end{aligned} \tag{33}$$

Substituting (16) into (26a) and using (33) to simplify the result yields

$$u_\ell^{(\mathrm{e})}(x) = \frac{\epsilon_\ell'}{4}\left[\left|\Gamma_\ell^+(x)\right|^2 + \left|\Gamma_\ell^-(x)\right|^2 + 2\mathrm{Re}\left[\Gamma_\ell^+(x)\Gamma_\ell^{-*}(x)\right]\right]. \tag{34}$$

Substituting (17) into (26b) and using (33) to simplify the result yields

$$u_\ell^{(\mathrm{m})}(x) = \frac{\mu_\ell' |w_\ell|^2}{4}\left[\left(1 + \frac{k_{y,p}^2}{|k_{x,\ell}|^2}\right)\left(\left|\Gamma_\ell^+(x)\right|^2 + \left|\Gamma_\ell^-(x)\right|^2\right) - 2\left(1 - \frac{k_{y,p}^2}{|k_{x,\ell}|^2}\right)\mathrm{Re}\left[\Gamma_\ell^+(x)\Gamma_\ell^{-*}(x)\right]\right], \tag{35}$$

where w_ℓ is given by (19).

7. Transmission and reflection coefficients

The transmission coefficient, T, and the reflection coefficient, R, are given by

$$T = \frac{\mathrm{Re}\left[\mathbf{S}_0^+\right]\cdot\hat{\mathbf{x}}}{\mathrm{Re}\left[\mathbf{S}_p^+\right]\cdot\hat{\mathbf{x}}}, \tag{36a}$$

$$R = -\frac{\mathrm{Re}\left[\mathbf{S}_p^-\right]\cdot\hat{\mathbf{x}}}{\mathrm{Re}\left[\mathbf{S}_p^+\right]\cdot\hat{\mathbf{x}}}, \tag{36b}$$

with

$$\mathbf{S}_0^+ = \frac{1}{2}\mathbf{E}_0^+ \times \mathbf{H}_0^{+*} \quad \text{and} \quad \mathbf{S}_p^\pm = \frac{1}{2}\mathbf{E}_p^\pm \times \mathbf{H}_p^{\pm *},$$

where it is understood that $\mathbf{E}_p^\pm$ and $\mathbf{H}_p^{\pm *}$ are evaluated at the interface between regions p and $p-1$ (the interface is approached from region p), and $\mathbf{E}_0^+$ and $\mathbf{H}_0^{+*}$ are evaluated at the interface between regions 1 and 0 (the interface is approached from the 0th region).

In the case of the parallel polarization state, substituting (11) and (12) into (36), and using (13) to simplify the result, yields

$$T = \frac{k_{x,p}}{\epsilon_p}\frac{\mathrm{Re}\left[\epsilon_0^* k_{x,0}\right]}{|k_{x,0}|^2}\left|\frac{\chi_0^+}{\chi_p^+}\right|^2, \tag{37a}$$

$$R = \left|\frac{\chi_p^-}{\chi_p^+}\right|^2. \tag{37b}$$

In the case of the perpendicular polarization state, substituting (17) and (16) into (36), and using (18) to simplify the result, yields

$$T = \frac{\mu_p}{k_{x,p}}\mathrm{Re}\left[\frac{k_{x,0}^*}{\mu_0^*}\right]\left|\frac{\chi_0^+}{\chi_p^+}\right|^2, \tag{38a}$$

$$R = \left|\frac{\chi_p^-}{\chi_p^+}\right|^2. \tag{38b}$$

Table 1
The first column contains the name (as it appears in the code) of the object attribute (method) of the class `Layer`, the second column contains a description of the method, and the third column contains references to the section where a more detailed description may be found.

Name	Description	Refs.
`field`	Transverse component of the electric field as a function of distance, $\Gamma^{\pm}(x)$	6.1, 6.2
`energy`	Electric/magnetic energy density as a function of distance, $u^{(e,m)}(x)$	6.1, 6.2
`loss`	Electric/magnetic losses as a function of distance, $Q^{(e,m)}(x)$	6
`divPoynting`	Divergence of the Poynting vector as a function of distance, $\nabla \cdot \mathbf{S}(x)$	6
`FIM`	FIM at each boundary interface	6
`FIMvsDist`	FIM as a function of distance	6
`TRvsFreq`	Transmission and reflection coefficients as a function of frequency $f = \omega/2\pi$ and/or angle of incidence ϕ,	7
`TRvsAngle`	i.e., $\{T(f), R(f)\}$, $\{T(\phi), R(\phi)\}$, $\{T(f,\phi), R(f,\phi)\}$	
`TRvsFreqAndAngle`		

Table 2
The first column contains the name (as it appears in the code) of the object attribute of the class `Boundary`, the second column contains a description of the attribute, and the third column contains references to a section and/or equation where a more detailed description of the attribute may be found.

Name	Description	Refs.
`self.h`	Thickness of each layer, h_ℓ	(13), (18)
`self.epsRel`	Relative permittivity of each region, $\epsilon_\ell/\epsilon_{\text{vacuum}}$	Section 3
`self.muRel`	Relative permeability of each region, $\mu_\ell/\mu_{\text{vacuum}}$	Section 3
`self.pol`	Polarization state	Section 4
`self.kx`	x-component of the wavevector, $k_{x,\ell}$	(8)
`self.w`	Scaled `self.kx` (polarization dependent), w_ℓ	(15), (19)
`self.chiPlus`	Transverse component of the electric field evaluated on the interface, χ^+_ℓ/χ^+_p	(13), (18)
`self.chiMinus`	Transverse component of the electric field evaluated on the interface, χ^-_ℓ/χ^+_p	(13), (18)

The transmission and reflection coefficients, given by (37) for the parallel polarization state and by (38) for the perpendicular polarization state, are valid for both a right- and a left-handed material.

8. Multilayer classes

Python is a multi-paradigm programing language that supports object-oriented programing, structured programing, and a subset of functional and aspect-oriented programing styles. There is a large number of numerical libraries available for use with Python. We chose to use a numerical library called SciPy [42] for numerical computations because, in our opinion, a reader familiar with MATLAB™ and/or Fortran 90/95 will find SciPy a very natural and easy-to-use library.

In order for our multilayer classes, namely `Boundary` and `Layer`, which are collectively called `openTMM`,[4] to be as useful as possible to the scientific community, we paid particular attention to the readability, usability, and maintainability of the code. Both classes are implemented in an object-oriented programing style as described below.

The `Boundary` class is meant to be a base class (*superclass* in the Python lexicon) that will be inherited by the derived classes (*subclasses* in the Python lexicon). The derived classes perform "high-level" computations such as computing the energy density and the transmission and reflection coefficients. The derived `Layer` class inherits the `Boundary` and computes the quantities described in Table 1. The benefit of using inheritance in our multilayer calculations is that other developers may extend the `Layer` class or write their own derived class to compute the desired quantity of interest without having to implement the low-level code, e.g., the code for computing $k_{x,\ell}$ and the S-matrix. The `Boundary` superclass computes a "minimal" set of "basic" quantities, see Table 2, that are used by the `Layer` subclass. Each function/method in the `Boundary` and `Layer` class contains a documentation header (*docstring* in the Python lexicon), which describes the function/method in detail and includes an example of its use. To access the docstrings, the user may use Python's `help` function or if more user friendly formatting is desired, the user may use SciPy's `info` function. For example, the docsting for `Layer.energy` function may be accessed via.

```
>>> help(openTMM.Layer.energy)
>>> scipy.info(openTMM.Layer.energy)
```

and all docstings contained in a class may be accessed via

```
>>> help(openTMM.ClassName)
>>> scipy.info(openTMM.ClassName)
```

[4] `openTMM` is an open-source software distributed under the MIT license and is available from http://pypi.python.org/pypi/openTMM.

where `ClassName` is either `Boundary` or `Layer`. This interactive documentation feature of Python makes it a very convenient language to use and largely eliminates the need to produce separate code documentation. The `help/scipy.info` functions are similar to the *Manual pager utils* (man pages) of Unix-like operating systems; could one imagine using a Linux shell without `man python`?

9. Python and numerical efficiency

There is some concern about the speed of computations in Python because it is *byte-compiled*, not a compiled language such as Fortran 90/95 or C/C++. However, in our opinion, the code readability (less error-prone syntax), flexibility (effortless integration with other software) and ease-of-use of Python (leading to shorter development times) in many cases outweigh any performance benefits of compiled languages. An interested reader may consult [43–46] for a fuller discussion of why Python is a language of choice for scientific software development. Typically, computationally intensive routines in Python are implemented in compiled languages and therefore, the difference in computation time between Python and complied languages is acceptable for many applications [44–47]. In the Python lexicon, the mixing of programing languages is called the *Pythonic approach*; this is the approach we use with the computationally intensive part of the `Boundary` superclass.

It is relatively obvious that the computationally intensive part of the `Boundary` superclass is the computation of $\chi_\ell^{\pm}$, i.e., the solution of the linear system described in Section 5. Therefore, the computation of $\chi_\ell^{\pm}$ is implemented in Fortran 90 and the Python bindings are built by F2PY [48] (F2PY is now part of SciPy). However, implementing "workhorse functions" in a compiled language reduces the readability and maintainability of code to some extent. Therefore, we strongly encourage developers to only implement workhorse functions in compiled languages when they lead to severe bottlenecks. It is often the case that bottlenecks can only be identified after code profiling (performance analysis). For example, it is not obvious that the square root function in the computation of $k_{x,\ell}$ is relatively time-consuming. The computation of $k_{x,\ell}$ is relatively expensive because SciPy's square root function, `scipy.sqrt`, does an element-by-element analysis of the input array to find if it contains any real elements less than zero. If a real, less-than-zero element is found, SciPy converts the whole input array to a complex data type and passes it to NumPy [49], which uses an efficient C code to compute the square root. In our case, SciPy's time-consuming element-by-element analysis is unnecessary because of a priori knowledge about $k_{x,\ell}$, see Section 3. We could avoid `scipy.sqrt` by directly using NumPy's square root function, but this is not the most convenient approach because NumPy's square root function of a complex number $z = |z|e^{i\theta}$ returns $\sqrt{|z|}e^{i\theta/2}$, where $-\pi < \theta \leqslant \pi$, but (8) requires that $\mathrm{Im}[k_{x,\ell}] > 0$. To avoid this inconvenience, we choose to implement our own square root subroutine, `cmplx_sqrt`, which returns the square root in an appropriate quadrant as required by (8). The `cmplx_sqrt` is implemented in Fortran 90 with Python binding build by F2PY and depends on Fortran's intrinsic square root function, `SQRT`.

To confirm that the run-time of the Python `Boundary` superclass is acceptable, we compared it to a `Boundary` class implemented in pure Fortran 90. From Fig. 2, we see that for a large number of layers ($\gtrsim 300$) the Python code is only 25 percent slower than the pure Fortran 90 code. However, for a small number of layers ($\lesssim 20$) the Python code is about 10 times slower than the pure Fortran 90 code, see inset in Fig. 2, but this is not major concern because such a small number of layers has an absolute execution time about a second or so in Python. We believe that the run-time discrepancy between a small and a large number of layers is caused by SciPy's overhead cost, which does not increase significantly as a function of array size.

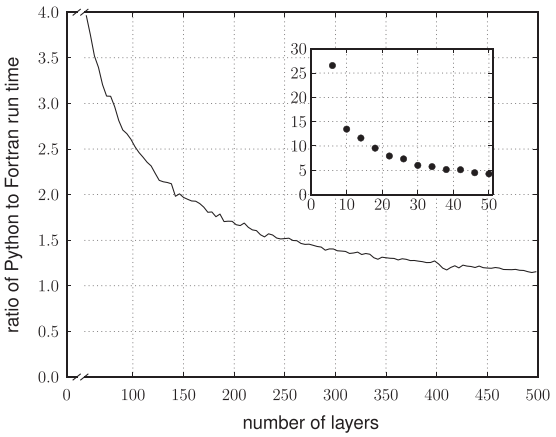

Fig. 2. The ratio of total computational time required to compute $T(f_i, \phi_j)$ and $R(f_i, \phi_j)$, where $1 \leqslant \{i,j\} \leqslant 10^3$, using `openTMM` and a pure Fortran 90 code. Each multilayer stack is composed of the same number of pseudorandom layers of the following types: right-handed layers with/without absorption and left-handed layers with/without absorption.

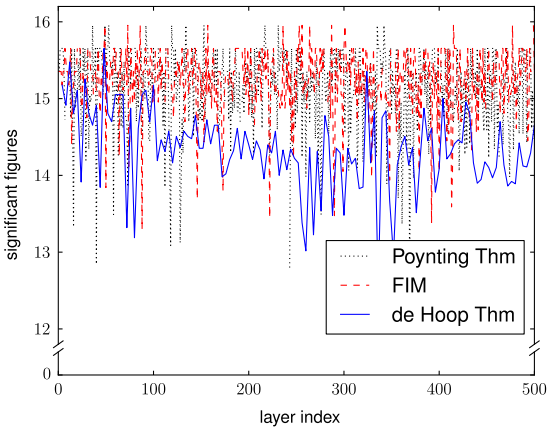

Fig. 3. $\delta_\tilde{\nu}$ is shown for a multilayer stack composed of the same number of pseudorandom layers of the following types: right-handed layers with/without absorption and left-handed layers with/without absorption.

10. Numerical stability and accuracy

To demonstrate the numerical stability and accuracy of `openTMM`, we numerically checked the complex Poynting theorem given by (25a), the fundamental invariant in multilayers given by (27), and the de Hoop reciprocity theorem [50, Section 6]. The de Hoop reciprocity theorem states that if $\epsilon_0 = \epsilon_p$ and $\mu_0 = \mu_p$, then the transmitted wave is unaffected by a 180 degree rotation of the multilayer stack around the z-axis, see Fig. 1. We measure the accuracy of a computed quantity in terms of the number of significant digits it agrees with the theoretical value and we denote this measure of accuracy by δ_ν. Approximately, δ_ν is given by

$$\delta_\tilde{\nu} \approx \min\left\{-\log\left|\frac{\nu-\tilde{\nu}_{\mathrm{Re}}}{\nu}\right|, -\log\left|\frac{\nu-\tilde{\nu}_{\mathrm{Im}}}{\nu}\right|\right\}, \tag{39}$$

where ν is the theoretical value and $\{\tilde{\nu}_{\mathrm{Re}}, \tilde{\nu}_{\mathrm{Im}}\}$ are the numerically computed value. For a numerical check of the complex Poynting theorem $\tilde{\nu}_{\mathrm{Re}}$ is given as $-\mathrm{Re}[\nabla\cdot\mathbf{S}]/[Q^{(\mathrm{e})}+Q^{(\mathrm{m})}]$ and $\tilde{\nu}_{\mathrm{Im}}$ is given as $-\mathrm{Im}[\nabla\cdot\mathbf{S}]/[2\omega(u^{(\mathrm{e})}-u^{(\mathrm{m})})]$. For the FIM test, $\tilde{\nu}_{\mathrm{Re}}(\tilde{\nu}_{\mathrm{Im}})$ is the ratio of the the real (imaginary) part of the left-hand side to the real (imaginary) part of the right-hand side of (27). For the de Hoop reciprocity test, $\tilde{\nu}_{\mathrm{Re}} = \mathrm{Re}[\chi_0^+]/\mathrm{Re}[\chi_p^+]$ and $\tilde{\nu}_{\mathrm{Im}} = \mathrm{Im}[\chi_0^+]/\mathrm{Im}[\chi_p^+]$, where χ_0^+ is the transmitted wave before the 180 degree rotation of the multilayer stack and χ_p^+ is the transmitted wave after the rotation. For all three numerical checks, $\nu = 1$ and all computations are performed in double-precision ($\approx$16 significant digits). From Fig. 3, we see that the three numerical checks are satisfied with an accuracy of $\delta_\tilde{\nu} \geqslant 12$. Despite the fact that some of the layers in the stack chosen for Fig. 3 have very high absorption, $\mathrm{Im}[k_{x,\ell}\, h_\ell] \approx 30$, we see that $\delta_\tilde{\nu}$ does not decrease as a function of distance into the stack, which confirms that our S-matrix algorithm is indeed numerically stable. The composition of the multilayer stack is summarized in Table 3. To produce Fig. 3, we used a normally incident plane wave of frequency 100 GHz and the first pathological case scheme, see Section 3.2.

Table 3
The height, h, relative permittivity, ϵ_{rel}, and the relative permeability, μ_{rel}, of each layer were pseudorandomly chosen from the intervals shown in the table. E.g., from the second line of the table, we see that *125* layers have thickness between 1 mm and 10 mm, and relative permittivity/permeability between -10 and -1. A 500-layer stack was used for the Poynting theorem and the FIM test. For the de Hoop reciprocity theorem test, a multilayer stack consisting of $5, 9, 13, \ldots, 501$ layers was used.

Test	# of layers	h(mm)	ϵ'_{rel}	$\epsilon''_{\mathrm{rel}}$	μ'_{rel}	μ''_{rel}
Poynting theorrem & FIM	125	[1,10]	[1,10]	0	[1,10]	0
	125	[1,10]	[−10,−1]	0	[−10,−1]	0
	125	[1,10]	[−10,−1]	[0.01,0.1]	[−10,−1]	0
	115	[1,10]	[1,10]	0	[1,10]	[0.01,0.1]
	10	[10,15]	[2,10]	[0,2]	[1,10]	0
de Hoop theorem	{1,...,125}	[1,10]	[1,10]	0	[1,10]	0
	{1,...,125}	[1,10]	[−10,−1]	0	[−10,−1]	0
	{1,...,125}	[1,10]	[−10,−1]	[0.01,0.1]	[−10,−1]	0
	{1,...,125}	[1,10]	[1,10]	0	[1,10]	[0.01,0.1]
	1	[1,10]	[2,10]	[0,1]	[1,10]	0

11. Conclusions

A numerically stable S-matrix algorithm for electromagnetic wave propagation through planar stratified media composed of a right-handed and/or left-handed material has been implemented in Python. Pathological cases caused by an unphysical approximation of zero absorption have been carefully examined and numerically circumvented (see Section 3.2). The numerical computations were implemented in an object-oriented programing style by dividing them into two classes, `Boundary` and `Layer`. The `Boundary` class performs computationally intensive calculations, namely the solution of the linear system described in Section 5.1 and the square root of $k_{x,\ell}^2$. The workhorse functions of the `Boundary` class were implemented in Fortran 90 in order to avoid computational bottlenecks. The `Layer` class performs high-level calculations, such as calculation of $u^{(e,m)}(x)$, $Q^{(e,m)}(x)$, $\Gamma^{\pm}(x)$, and FIM. The code has been tested and is accurate to ≈ 12 significant digits (see Section 10).

We hope that our open-source and object-oriented implementation of the S-matrix algorithm, which is suitable for modern applications such as Anderson localization of light and perfect lensing, will be adopted by a wide scientific community. At the very least, we hope that our publicly available implementation of the S-matrix algorithm will encourage the scientific community to use open-source software, thus increasing the reproducibility of scientific work.

Acknowledgment

This work was partially supported by the U.S. Department of Energy under Grant DE-FG02–09ER16018. Also, this material is based upon work supported in part by the U.S. Office of Naval Research as a Multi-disciplinary University Research Initiative on Sound and Electromagnetic Interacting Waves under Grant No. N00014–10-1–0958.

References

[1] L.M. Brekhovskikh, Waves in Layered Media (Translated from Russian by David Lieberman), Academic Press, New York, 1960.
[2] J.R. Wait, Electromagnetic Waves in Stratified Media, IEEE Press, New York, 1996.
[3] J.M. Vigoureux, Polynomial formulation of reflection and transmission by stratified planar structures, J. Opt. Soc. Am. A 8 (1991) 1697–1701.
[4] T. El-Agez, S. Taya, A. El Tayyan, A polynomial approach for reflection, transmission, and ellipsometric parameters by isotropic stratified media, Opt. Appl. 40 (2010) 501–510.
[5] J.M. Vigoureux, Use of Einstein's addition law in studies of reflection by stratified planar structures, J. Opt. Soc. Am. A 9 (1992) 1313–1319.
[6] J.J. Monzón, L.L. Sánchez-Soto, Fully relativisticlike formulation of multilayer optics, J. Opt. Soc. Am. A 16 (1999) 2013–2018.
[7] P. Grossel, J.M. Vigoureux, F. Baïda, Nonlocal approach to scattering in a one-dimensional problem, Phys. Rev. A 50 (1994) 3627–3637.
[8] R.L. Mooney, An exact theoretical treatment of reflection-reducing optical coatings, J. Opt. Soc. Am. 35 (1945) 574–583.
[9] W. Weinstein, The reflectivity and transmissivity of multiple thin coatings, J. Opt. Soc. Am. 37 (1947) 576–577.
[10] F. Abelès, La théorie générale des couches minces, J. Phys. Radium 11 (1950) 307–310.
[11] M. Born, E. Wolf, Principles of Optics: Electromagnetic Theory of Propagation, Interference and Diffraction of Light, sixth (corrected) ed., Pergamon Press, Oxford, 1986.
[12] E.L. Tan, Enhanced R-matrix algorithms for multilayered diffraction gratings, Appl. Opt. 45 (2006) 4803–4809.
[13] F. Montiel, M. Nevière, Differential theory of gratings: extension to deep gratings of arbitrary profile and permittivity through the R-matrix propagation algorithm, J. Opt. Soc. Am. A 11 (1994) 3241–3250.
[14] L. Li, Multilayer modal method for diffraction gratings of arbitrary profile, depth, and permittivity, J. Opt. Soc. Am. A 10 (1993) 2581–2591.
[15] L. Li, Formulation and comparison of two recursive matrix algorithms for modeling layered diffraction gratings, J. Opt. Soc. Am. A 13 (1996) 1024–1035.
[16] M. Auslender, S. Hava, Scattering-matrix propagation algorithm in full-vectorial optics of multilayer grating structures, Opt. Lett. 21 (1996) 1765–1767.
[17] N.P.K. Cotter, T.W. Preist, J.R. Sambles, Scattering-matrix approach to multilayer diffraction, J. Opt. Soc. Am. A 12 (1995) 1097–1103.
[18] D. Yuk Kei Ko, J.R. Sambles, Scattering matrix method for propagation of radiation in stratified media: attenuated total reflection studies of liquid crystals, J. Opt. Soc. Am. A 5 (1988) 1863–1866.
[19] D. Yuk Kei Ko, J.C. Inkson, Matrix method for tunneling in heterostructures: resonant tunneling in multilayer systems, Phys. Rev. B 38 (1988) 9945–9951.
[20] V.G. Veselago, The electrodynamics of substances with simultaneously negative values of ϵ and μ, Sov. Phys. Uspekhi 10 (1968) 509–514.
[21] D.R. Smith, W.J. Padilla, D.C. Vier, S.C. Nemat-Nasser, S. Schultz, Composite medium with simultaneously negative permeability and permittivity, Phys. Rev. Lett. 84 (2000) 4184–4187.
[22] R.A. Shelby, D.R. Smith, S. Schultz, Experimental verification of a negative index of refraction, Science 292 (2001) 77–79.
[23] S.A. Ramakrishna, Physics of negative refractive index materials, Rep. Prog. Phys. 68 (2005) 449–521.
[24] J.B. Pendry, Negative refraction makes a perfect lens, Phys. Rev. Lett. 85 (2000) 3966–3969.
[25] M. Scalora, G. D'Aguanno, N. Mattiucci, M.J. Bloemer, D. de Ceglia, M. Centini, A. Mandatori, C. Sibilia, N. Akozbek, M.G. Cappeddu, M. Fowler, J.W. Haus, Negative refraction and sub-wavelength focusing in the visible range using transparent metallo-dielectric stacks, Opt. Exp. 15 (2007) 508–523.
[26] E. Abrahams (Ed.), 50 Years of Anderson Localization, World Scientific, New Jersey, 2010.
[27] P. Sheng, Introduction to Wave Scattering, Localization and Mesoscopic Phenomena, second ed., Springer, Berlin, 2006.
[28] J.A. Scales, L.D. Carr, D.B. McIntosh, V. Freilikher, Y.P. Bliokh, Millimeter wave localization: slow light and enhanced absorption in random dielectric media, Phys. Rev. B 76 (2007) 085118.
[29] K.Y. Bliokh, V.D. Freilikher, Localization of transverse waves in randomly layered media at oblique incidence, Phys. Rev. B 70 (2004) 245121.
[30] A.A. Asatryan, S.A. Gredeskul, L.C. Botten, M.A. Byrne, V.D. Freilikher, I.V. Shadrivov, R.C. McPhedran, Y.S. Kivshar, Anderson localization of classical waves in weakly scattering metamaterials, Phys. Rev. B 81 (2010) 075124.
[31] R. Giust, J.M. Vigoureux, M. Sarrazin, Asymmetrical properties of the optical reflection response of the Fabry–Pérot interferometer, J. Opt. Soc. Am. A 17 (2000) 142–148.
[32] S.V. Zhukovsky, Perfect transmission and highly asymmetric light localization in photonic multilayers, Phys. Rev. A 81 (2010) 053808.
[33] L.D. Landau, E.M. Lifshitz, Statistical Physics: Part 1 (Translated from Russian by J.B. Sykes and M.J. Kearsley), vol. 5, Pergamon Press, Oxford, third revised and enlarged edition, 1993.
[34] L.D. Landau, E.M. Lifshitz, P.L.Petrovich, Electrodynamics of Continuous Media (Translated from Russian by J.B. Sykes, M.J. Kearsley and J.S. Bell), vol. 8, Pergamon Press, Oxford, second revised and enlarged edition, 1993.
[35] J. Skaar, On resolving the refractive index and the wave vector, Opt. Lett. 31 (2006) 3372–3374.

[36] J.A. Stratton, Electromagnetic Theory, McGraw-Hill, New York, 1941.
[37] R. Ruppin, Electromagnetic energy density in a dispersive and absorptive material, Phys. Lett. A 299 (2002) 309–312.
[38] A.M. Vadim, Correct definition of the Poynting vector in electrically and magnetically polarizable medium reveals that negative refraction is impossible, Opt. Exp. 16 (2008) 19152–19168.
[39] J.M. Vigoureux, P. Grossel, A relativistic-like presentation of optics in stratified planar media, Am. J. Phys. 61 (1993) 707–712.
[40] J.M. Vigoureux, R. Giust, New relations in the most general expressions of the transfer matrix, Opt. Commun. 186 (2000) 21–25.
[41] R. Giust, J.M. Vigoureux, J. Lages, Generalized composition law from 2×2 matrices, Am. J. Phys. 77 (2009) 1068–1073.
[42] E. Jones, T. Oliphant, P. Peterson et al., SciPy: open source scientific tools for Python, 2001.
[43] L. Prechelt, An empirical comparison of seven programming languages, Computer 33 (2000) 23–29.
[44] E. Lambert, M. Fiers, S. Nizamov, M. Tassaert, S.G. Johnson, P. Bienstman, W. Bogaerts, Python bindings for the open source electromagnetic simulator Meep, Comput. Sci. Eng. 13 (2011) 53–65.
[45] O. Bröker, O. Chinellato, R. Geus, Using Python for large scale linear algebra applications, Future Gener. Comput. Sys. 21 (2005) 969–979.
[46] C. Rickett, S.-E. Choi, C. Rasmussen, M. Sottile, Rapid prototyping frameworks for developing scientific applications: a case study, J. Supercomput. 36 (2006) 123–134.
[47] L. Dalcín, R. Paz, M. Storti, MPI for Python, J. Parallel Distrib. Comput. 65 (2005) 1108–1115.
[48] P. Peterson, F2PY: a tool for connecting Fortran and Python programs, Int. J. Comput. Sci. Eng. 4 (2009) 296–305.
[49] T.E. Oliphant, Guide to NumPy, Provo, UT, 2006.
[50] R.J. Potton, Reciprocity in optics, Rep. Prog. Phys. 67 (2004) 717–754.
[51] A. Markushevich, Theory of Functions of a Complex Variable 3 volumes in one, translated from Russian by Richard A. Silverman, second ed., Chelsea Publishing Company, New York, 1977.